

Burst particle creation in gravitational collapse to a horizonless compact object

Takafumi Kokubu* and Tomohiro Harada†

Department of Physics, Rikkyo University, Toshima, Tokyo 171-8501, Japan

(Dated: May 29, 2019)

Abstract

In the previous paper [Harada, Cardoso, and Miyata, Phys. Rev. D **99** (2019), 044039], it is shown that a hollow transmissive shell collapsing to an ultracompact object of radius very close to its horizon radius generally emits transient Hawking radiation (THR) followed by a couple of bursts separated each other by a long time interval. In the current paper, we expand the previous work in two independent directions: changing boundary conditions and specifying the equations of state (EOSs) of the matter. First, we introduce a perfectly reflective surface collapsing to an ultracompact object and find that this model also emits THR that is followed only by a single burst. Second, we introduce two different collapse dynamics to an ultracompact object and specify the corresponding matter EOSs. We find that THR is quite commonly seen in early times, while the subsequent bursts strongly depend on the boundary condition and the EOS or the braking behavior of the surface.

PACS numbers: 04.70.Dy, 04.62.+v

arXiv:1905.07981v2 [gr-qc] 28 May 2019

* 14ra002a@rikkyo.ac.jp

† harada@rikkyo.ac.jp

CONTENTS

I. Introduction	3
II. Particle creation from a spherically symmetric star	5
III. Transient Hawking radiation	8
IV. Particle creation: a qualitative analysis	9
A. Phases of collapse dynamics	9
B. Post-Hawking burst	10
C. Time dependence of particle creation	11
1. Model A: exponentially slowed-down model	11
2. Model B: constant-deceleration model	12
V. Concrete dynamical models	12
A. Pure $p = w\rho$ model	13
B. Hybrid $p = w\rho$ model	15
C. Hybrid quadratic model	17
VI. Particle creation: a numerical analysis	18
A. Hybrid $p = w\rho$ transmissive model	18
B. Hybrid quadratic transmissive model	19
C. Hybrid $p = w\rho$ reflective model	22
D. Hybrid quadratic reflective model	24
VII. Discussion and conclusion	25
Acknowledgments	27
A. Junction conditions	28
References	29

I. INTRODUCTION

In the current development of observational and theoretical astronomy and astrophysics, there is no doubt that black holes play a central role. The LIGO and Virgo terrestrial interferometric gravitational wave detectors have directly observed gravitational waves from binary black holes of tens of solar masses and confirmed the correctness of general relativity with high accuracy in such a strong field of gravity [1, 2]. More recently, the Event Horizon Telescope has succeeded in imaging the “shadow” of a central massive object of M87 as a powerful evidence for the existence of a supermassive black hole there [3]. On the other hand, these tremendous successes of astronomical observation turn the attention of researchers to a profound question on the nature of the black hole. What is the most decisive character and signature to distinguish a black hole from possible horizonless dark compact massive objects of radius R slightly larger than the horizon radius, $2GM/c^2$, where M is the mass of the object? See Cardoso and Pani [4] for a recent review on horizonless dark compact objects and references therein. See also [5–8]. A black hole is defined by an event horizon, which is the intersection of the past boundary of the future null infinity with the spacetime itself. By this definition, the black hole can never be observed by a distant observer or an observer outside the black hole. This means that even if an observer infers the existence of something very massive in a highly compact region without any signal of emission from itself, she or he can never conclude within a finite time that there is an event horizon or a black hole, as is clearly demonstrated in [9]. What the observer outside the horizon can do is to accumulate null results for the existence of a horizonless compact object as long as possible. This is the strongest evidence of a black hole that the observer can ever obtain in principle in classical physics.

In quantum field theory, however, the situation can be very different because the Hawking radiation [10, 11] can be regarded as the positive signature of a black hole. One might think that the existence of a black hole can be directly tested by the detection of the Hawking radiation, which is nearly black-body radiation of all possible degrees of freedom with temperature $T = T_H := c^3\hbar/(8\pi kGM)$. In the previous work [12] (hereafter Paper I), the authors have addressed this fundamental issue. Using a hollow transmissive spherical shell, they showed that a collapsing body can emit temporarily thermal radiation with $T = T_H$ during a finite time as if it is Hawking radiation, even though the collapse does not lead to the formation of any kind of horizon but to the formation of an ultracompact horizonless object. They call this radiation transient Hawking radiation (THR). The time evolution of radiation deviates from the standard Hawking radiation when the collapse is significantly slowed down. The typical feature of the radiation history after

the THR is a couple of bursts, the first immediately after the THR and the second very long after the first. We should note that the collapse model of a hollow transmissive spherical shell provides an unique probe into quantum field theory in gravitational collapse spacetimes as demonstrated in Refs. [13–15].

In the current paper, we expand the analysis in Paper I [12] in two independent directions. The first direction is to study a different boundary condition. Here, besides the transmissive boundary condition, we introduce a perfectly reflective boundary condition at the surface of the collapsing body. In this case, we do not have to specify the interior of the surface because the quantum field does not propagate in the interior region. Hence, we can think that it is filled with matter as a usual astrophysical star. We might heuristically regard the transmissive boundary condition as that for gravitational waves, while the reflective boundary condition as that for electromagnetic waves against a conductive surface. The second direction is to think the matter of the hollow shell. Because such a static ultracompact object needs to be supported against highly relativistic strong gravity, the matter field must have very strong pressure. We address what kind of equation of state (EOS) can explain the assumed collapse dynamics to an ultracompact object.

The organization of this paper is as follows. In Sec. II, we present the result of the application of quantum field theory in curved spacetime to an asymptotically flat spherically symmetric spacetime for both the transmissive and reflective boundary conditions. In Sec. III, we show that the THR is a common feature of the standard collapse with the radius very close to the horizon radius even if the collapse does not lead to the formation of any horizon. In Sec. IV, we introduce a collapse dynamics model to an ultracompact object and discuss that a single burst will be emitted after the THR in the case of the reflective boundary condition in contrast to a couple of bursts separated each other by a very long lapse of time in the transmissive case. In Sec. V, we present concrete dynamical models for the collapse to an ultracompact object in terms of the effective potential and the EOS of the matter on the shell. In Sec. VI, we present numerical results for particle creation in the concrete collapse models with both the transmissive and reflective boundary conditions and discuss that the numerical results can be well explained in terms of the qualitative analysis in Paper I [12] and in Sec. IV in the current paper. Section VII is devoted to summary and conclusion. We use the units in which $c = G = 1$ throughout the paper.

II. PARTICLE CREATION FROM A SPHERICALLY SYMMETRIC STAR

We calculate quantum particle creation in spherically symmetric asymptotically flat spacetimes. To do this, we adopt standard assumptions and approximations, including geometrical optics approximation, which are described in Paper I [12]. We just cite the result for the use in the current paper. The particle creation can be calculated by a mapping function G defined as $v_{\text{in}} = G(u_{\text{out}})$, where $u = u_{\text{out}}$ and $v = v_{\text{in}}$ are the observer's outgoing null coordinate and its corresponding ingoing null coordinate, respectively, in terms of the standard double null coordinates u and v in the asymptotic region. The function G depends on the boundary condition as we will see below. The total power of radiation is given by [16, 17]

$$P \simeq \frac{1}{48\pi}(\kappa^2 + 2\delta\kappa'), \quad (2.1)$$

with $\delta = 1$ and 0 for minimally and conformally coupled massless scalars, respectively, where $' := d/du$ and $\kappa(u)$ is defined as [18, 19]

$$\kappa(u) := -(\ln G)'. \quad (2.2)$$

We will omit the second term in the parentheses in Eq. (2.1) because it does not contribute to the integrated energy of radiation. This omission leads to the calculation of the power for the conformally coupled massless scalar field. If the function $\kappa(u_*)$ is positive and satisfies the adiabatic condition $|\kappa'(u_*)| \ll \kappa^2(u_*)$, then the spectrum of outgoing particles at $u = u_*$ can be regarded as thermal with temperature $T(u_*)$ such that [18, 19]

$$kT(u_*) = \frac{\kappa(u_*)}{2\pi}. \quad (2.3)$$

The function $\kappa(u)$ depends not only on the dynamics of the spacetime but also the boundary conditions of the stellar surface. In Paper I [12], the authors consider a situation where a hollow spherical shell which is perfectly transmissive to scalar waves collapses in vacuum. In this case, $G'(u)$ and $\kappa(u)$ are given by

$$G'(u) = \frac{A(\tau_{\text{out}})}{B(\tau_{\text{in}})}, \quad \kappa(u) = C(\tau_{\text{out}}) - \frac{A(\tau_{\text{out}})}{B(\tau_{\text{in}})}D(\tau_{\text{in}}), \quad (2.4)$$

where $A(\tau)$, $B(\tau)$, $C(\tau)$, and $D(\tau)$ are given in terms of $R(\tau)$, $\dot{R}(\tau)$, and $\ddot{R}(\tau)$, where $r = R(\tau)$ is the radius of the shell as a function of the proper time τ of an observer staying at the surface, the dot denotes the derivative with respect to τ , and τ_{out} and τ_{in} are the values of τ at which the outgoing null ray $u = u_{\text{out}}$ and the ingoing null ray $v = v_{\text{in}}$ cross the surface, respectively, as shown

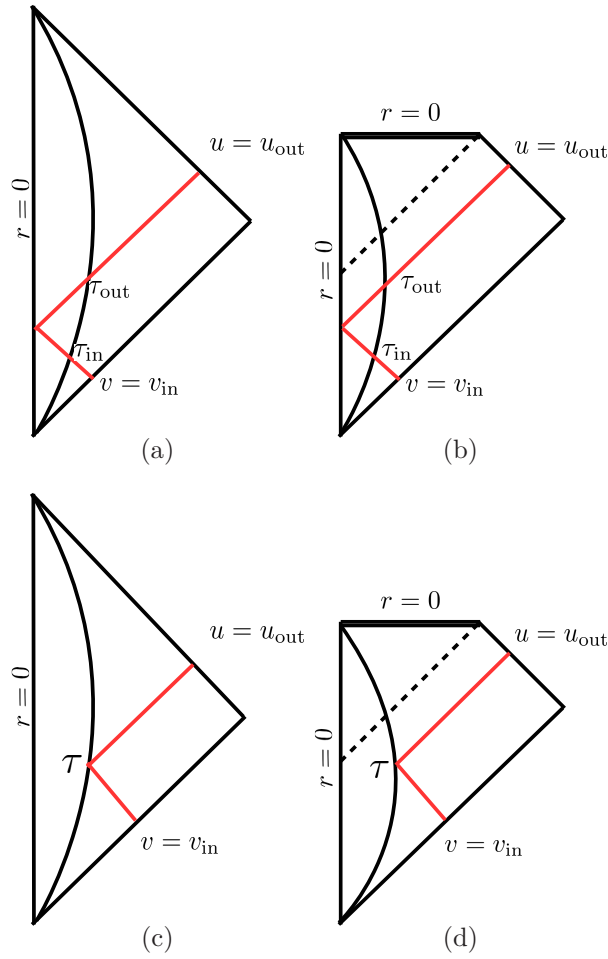


FIG. 1. The conformal diagrams for the spacetimes of collapse to a static star [(a) and (c)] and a black hole [(b) and (d)]. A pair of outgoing and ingoing null rays with $u = u_{\text{out}}$ and $v = v_{\text{in}}$ is depicted for a transmissive surface in (a) and (b), and for a reflective surface in (c) and (d).

in Fig. 1 (a) or (b). The explicit expressions for these functions are given in Appendix A of Paper I [12].

Next, we consider a situation where the stellar surface is perfectly reflective against scalar waves. We assume that the exterior is described by the Schwarzschild metric

$$ds^2 = - \left(1 - \frac{2M}{r}\right) dt^2 + \left(1 - \frac{2M}{r}\right)^{-1} dr^2 + r^2(d\theta^2 + \sin^2\theta d\phi^2), \quad (2.5)$$

while the metric in the interior of the star is left arbitrary. Defining

$$u = t - r^*, \quad v = t + r^*, \quad (2.6)$$

where $dr^* = dr/(1 - 2M/r)$, we find

$$\dot{u} = \frac{\sqrt{1 - \frac{2M}{R} + \dot{R}^2} - \dot{R}}{1 - \frac{2M}{R}}, \quad \dot{v} = \frac{\sqrt{1 - \frac{2M}{R} + \dot{R}^2} + \dot{R}}{1 - \frac{2M}{R}}, \quad (2.7)$$

from the junction condition of the first fundamental form, where τ is the value of τ at which the ingoing null ray $v = v_{in}$ is reflected by the surface to the outgoing null ray $u = u_{out}$ as seen in Fig. 1 (c) or (d). We do not need two proper times τ_{out} and τ_{in} but only τ in the reflective case. Then, we find

$$G'(u_{out}) = \frac{\dot{v}}{\dot{u}}(\tau), \quad \kappa(u) = \frac{1}{\dot{u}} \frac{d}{d\tau} \ln \frac{\dot{u}}{\dot{v}}(\tau). \quad (2.8)$$

Implementing the calculation, we find

$$G' = \frac{\sqrt{1 - \frac{2M}{R} + \dot{R}^2} + \dot{R}}{\sqrt{1 - \frac{2M}{R} + \dot{R}^2} - \dot{R}}, \quad \kappa = 2 \frac{\sqrt{1 - \frac{2M}{R} + \dot{R}^2} + \dot{R}}{\sqrt{1 - \frac{2M}{R} + \dot{R}^2}} \left(-\ddot{R} + \frac{M}{R^2} \frac{\dot{R}^2}{1 - \frac{2M}{R}} \right), \quad (2.9)$$

where the right-hand sides are evaluated at the retarded time τ and we omit it for brevity.

Therefore, only the state of the shell at the retarded time τ is responsible for particle creation at $u = u_{out}$ unlike in the transmissive case. If $M = 0$, Eq. (2.9) reduces to

$$\kappa = -2 \left(1 + \frac{\dot{R}}{\sqrt{1 + \dot{R}^2}} \right) \ddot{R}. \quad (2.10)$$

This corresponds to particle creation by a spherical moving mirror in the flat spacetime, which is comparable with a planar moving mirror in the flat spacetime discussed in [16]. If the surface is expanding with highly relativistic speed, i.e., $\dot{R} \gg 1$, then Eq. (2.9) reduces to

$$\kappa \simeq \frac{4M}{R^2 \left(1 - \frac{2M}{R}\right)} \Gamma^2 - 4\ddot{R}, \quad (2.11)$$

where $\Gamma := [1 - (dR/dt)^2]^{-1/2} = \sqrt{1 + \dot{R}^2}$. In the above, the first term gives an interesting effect: If $\Gamma \gg 1$, the first term can be very large and, hence, κ can be much greater than its Hawking value $\kappa_H = 1/(4M)$ independently from the acceleration even if $R > 2M$. On the other hand, if the surface is shrinking with highly relativistic speed, i.e., $-\dot{R} \gg 1$, then Eq. (2.9) reduces to

$$\kappa \simeq - \left(1 - \frac{2M}{R} \right) \frac{\ddot{R}}{\Gamma^2} + \frac{M}{R^2}. \quad (2.12)$$

Therefore, there is not enhancement but suppression on the first term due to a relativistic speed.

III. TRANSIENT HAWKING RADIATION

In Paper I [12], particle creation is calculated for a hollow transmissive shell. Here, we calculate particle creation for a perfectly reflective surface. First, we consider particle creation from standard collapse.

By the standard collapse, we refer to the following dynamics:

- 1) Phase 0, an early-collapse phase: $\tau < \tau_0$ or $u < u_0$.

We assume

$$1 - \frac{2M}{R} > \frac{1}{2}, \quad |\dot{R}| \lesssim 1, \quad \text{and} \quad |\ddot{R}| \lesssim \frac{1}{2M}. \quad (3.1)$$

- 2) Phase 1, a late-collapse phase: $\tau > \tau_0$ or $u > u_0$.

We assume

$$1 - \frac{2M}{R} < \frac{1}{2}, \quad 1 - \frac{2M}{R} < \dot{R}^2, \quad \dot{R} = O(1), \quad \text{and} \quad \ddot{R} = O((2M)^{-1}). \quad (3.2)$$

From Eq. (2.9), we can estimate $\kappa(u)$ as follows:

- 1) $u < u_0$

We have

$$\kappa(u) \simeq 2 \left[M \left(\frac{\dot{R}}{R} \right)^2 - \ddot{R} \right]. \quad (3.3)$$

Therefore, we can conclude that $|\kappa| \lesssim 1/(4M)$. Thus, the radiation for $u < u_0$, which may be called pre-Hawking radiation, is not much stronger than the standard Hawking radiation.

- 2) $u > u_0$

We have

$$\kappa(u) \simeq \frac{1}{4M}. \quad (3.4)$$

Since we can also see that the adiabatic condition is satisfied, the radiation is temporarily thermal with $kT = 1/(8\pi M)$. Therefore, there is THR also in the case of a reflective surface. Since THR is derived without assuming any horizon, we can conclude that THR does not need any horizon. If the late-collapse phase continues up until $R \simeq 2M(1+\epsilon^2)$, then the THR arises and lasts for $\Delta u \simeq 4M \ln \epsilon^{-2}$. In the limit $\epsilon \rightarrow 0$, the Hawking radiation continues eternally and the energy radiated goes to infinity.

These features are common to both transmissive and reflective cases.

IV. PARTICLE CREATION: A QUALITATIVE ANALYSIS

In Ref.[13] and Paper I [12], the authors consider a collapse model in which a static surface turns to an imploding null surface at $u = u_0$ and then to a static surface again at $u = u_1 > u_0$ under the transmissive condition, for which they find that the THR is derived fully analytically. In the reflective case, however, this model does not work. This is because in the imploding phase, $v_{in} = \text{const.}$ for $u_0 < u_{out} < u_1$ and, hence, $G' = 0$ for this range of u_{out} . Thus, we cannot obtain any meaningful function for $\kappa = -(\ln G)'$. For this reason, we concentrate on the timelike surface model. Since the transmissive condition is studied in detail in Paper I [12], we concentrate on the reflective case.

A. Phases of collapse dynamics

As in Paper I [12], we assume the following collapse dynamics, after which a static ultracompact object of radius $R = R_f = 2M(1 + \epsilon^2)$ is formed.

- 1) Phase 0, an early-collapse phase: $\tau < \tau_0$ or $R > 4M$.

We assume $1 - 2M/R > 1/2$, $|\dot{R}| \lesssim 1$, and $|\ddot{R}| \lesssim 1/(2M)$.

- 2) Phase 1, a late-collapse phase: $\tau_0 < \tau < \tau_1$ or $R_b < R < 4M$.

We assume $1 - 2M/R < 1/2$, $1 - 2M/R < \dot{R}^2$, $\dot{R} = O(1)$, and $\ddot{R} = O((2M)^{-1})$. We denote the end of the standard collapse with τ_1 and $R_b := R(\tau_1)$.

- 3) Phase 2, an early-braking phase: $\tau_1 < \tau < \tau_2$ or $R_2 < R < R_b$.

We assume that at $\tau = \tau_1$ or $R = R_b$, the surface begins to brake. For $\tau_1 < \tau < \tau_2$, we assume the following inequality:

$$1 - \frac{2M}{R} < \dot{R}^2. \quad (4.1)$$

- 4) Phase 3, a late-braking phase: $\tau_2 < \tau < \tau_3$ or $R_f < R < R_2$

We assume that at $\tau = \tau_2$, when $R = R_2$, the following equality holds:

$$1 - \frac{2M}{R} = \dot{R}^2. \quad (4.2)$$

For $\tau_2 < \tau < \tau_3$, the following inequality holds:

$$1 - \frac{2M}{R} > \dot{R}^2. \quad (4.3)$$

The radius approaches the final value R_f .

5) Phase 4, a final static phase: $\tau > \tau_3$ or $R = R_f$.

We assume that $R(\tau)$ smoothly reaches R_f at $\tau = \tau_3$. Later on, the surface is completely static.

Figure 2 depicts the situation, where we label as $u = u_0, u_1, u_2$, and u_3 those outgoing null rays in the Schwarzschild region which leave the surface outwardly at $\tau = \tau_0, \tau_1, \tau_2$, and τ_3 , respectively.

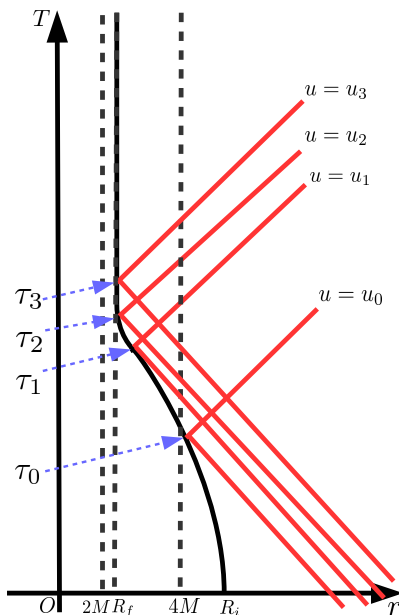


FIG. 2. The collapse model with a timelike surface. The surface enters $R = 4M$ at $\tau = \tau_0$, begins to brake at $\tau = \tau_1$, and stops at $\tau = \tau_3$. Between τ_1 and τ_3 , there is a moment τ_2 , when the equality $1 - 2M/R = \dot{R}^2$ is satisfied. The outgoing null rays which leave the surface outwardly to the Schwarzschild region at $\tau = \tau_0, \tau_1, \tau_2$, and τ_3 are denoted by red lines labeled $u = u_0, u_1, u_2$, and u_3 , respectively.

B. Post-Hawking burst

In Paper I [12], the authors show that in the transmissive case, there are a couple of bursts, the first one immediately after the THR and the second one long after the first. Here, we find that in the reflective case, there can appear only a single burst of radiation, which is immediately after the THR, in contrast to the transmissive case.

For $u_1 < u < u_3$, the observer receives an outgoing null ray which left the surface in the braking phase and can be traced back to the ingoing null ray which reaches the surface at the same time. The function $\kappa(u)$ is approximately given by

$$\kappa(u) \simeq -\frac{1 - \frac{2M}{R}}{\dot{R}^2} \ddot{R} + \frac{1}{4M}, \quad (4.4)$$

$$\kappa(u) \simeq -2\ddot{R} + \frac{2\dot{R}^2}{1 - \frac{2M}{R}} \frac{1}{4M}, \quad (4.5)$$

for $u_1 < u < u_2$ and $u_2 < u < u_3$, respectively. Note that the function $\dot{R}^2/(1 - \frac{2M}{R})$ is generally a decreasing function for $u_1 < u < u_3$, which is greater than unity at $u = u_1$, unity at $u = u_2$, and zero at $u = u_3$. In Eqs. (4.4) and (4.5), the second term can be regarded as the THR, which keeps constant for $u_1 < u < u_2$ and decays for $u_2 < u < u_3$. This implies that u_2 (or τ_2) plays a clear physical role: it triggers the interruption of THR. On the other hand, the first term, which is negative, dominates the second term if $\ddot{R} \gtrsim 1/(2M)$ at $\tau = \tau_2$ or $u = u_2$. The emission due to the first term completely ends at $u = u_3$. This gives a burst of radiation in the end of the THR around at $u = u_2$, which we call a post-Hawking burst. The details of the burst depend on the behavior of the surface in the braking phase. It is clear that in the reflective case, there is no further burst in contrast to the transmissive case.

C. Time dependence of particle creation

Here we analyze the time dependence of the power of radiation in detail for a couple of very simple braking models.

1. Model A: exponentially slowed-down model

First, we assume that $R - R_f \propto e^{-\sigma\tau}$ for $\tau_1 < \tau < \tau'_3$ by introducing the deceleration parameter σ such that $\ddot{R} = \sigma|\dot{R}| = \sigma^2(R - R_f)$ with

$$\sigma = \frac{|\dot{R}_b|}{R_b - R_f}, \quad (4.6)$$

where $|\dot{R}_b| = O(1)$. Then, for $\tau'_3 < \tau < \tau_3$, we assume that R smoothly settles down to the final fixed radius R_f at $\tau = \tau_3$. We parameterize σ such that

$$\sigma^{-1} = 2M\epsilon^{2\beta}, \quad (4.7)$$

where we assume $\beta \geq 1/2$. The dynamics of this model is described in detail in Paper I [12].

We can see that the first term for $u_1 < u < u_2$ on the right-hand side of Eq. (4.4) is negative and its absolute value increases and reaches $O(\epsilon^{1-2\beta}M^{-1}) = O(\epsilon\sigma)$ at $u = u_2$. The first term on the right-hand side of Eq. (4.5) then just decays to zero for $u_2 < u < u_3$. Therefore, the post-Hawking burst is much stronger than the THR at $u = u_2$ only if $\beta > 1/2$, while it is as strong as the THR if $\beta = 1/2$. The duration of the burst is given by $u_3 - u_1 \simeq 4M(1 - \beta) \ln \epsilon^{-2}$ for $1/2 \leq \beta < 1$, $\simeq 4M$ for $\beta = 1$, and $\simeq 4M\epsilon^{2(\beta-1)}$ for $\beta > 1$.

2. Model B: constant-deceleration model

Next we consider a technically simpler model, where the deceleration a of the surface is constant for $\tau_1 < \tau < \tau_3$ with

$$a = \frac{\dot{R}_b^2}{2(R_b - R_f)}, \quad (4.8)$$

where $|\dot{R}_b| = O(1)$. We can naturally assume $a \gg 1/(4M)$. We parameterize $a^{-1} = 2M\epsilon^{2\beta}$ as in the previous model. The dynamics of this model is described in detail in Paper I [12].

We can see that the first term on the right-hand side of Eq. (4.4) is negative and its absolute value increases for $u_1 < u < u_2$ and reaches $O(\epsilon^{-2\beta}M^{-1}) = O(a)$ at $u = u_2$. The first term on the right-hand side of Eq. (4.5) is then constant for $u_2 < u < u_3$. Therefore, the post-Hawking burst is much stronger than the THR for $u_2 < u < u_3$ only if $\beta > 0$, while it is as strong as the THR if $\beta = 0$. The duration of the burst is given by $u_3 - u_1 \simeq 4M(1 - \beta) \ln \epsilon^{-2}$ for $1/2 \leq \beta < 1$, $\simeq 4M$ for $\beta = 1$, and $\simeq 4M\epsilon^{2(\beta-1)}$ for $\beta > 1$.

V. CONCRETE DYNAMICAL MODELS

In this section, we introduce three concrete matter models for the collapsing surface. All of the models introduced here are categorized as model A in the previous section, i.e., the surface is exponentially slowed down in late times. Three effective potentials introduced in this section are summarized in Fig. 3. The details will be discussed below for each model.

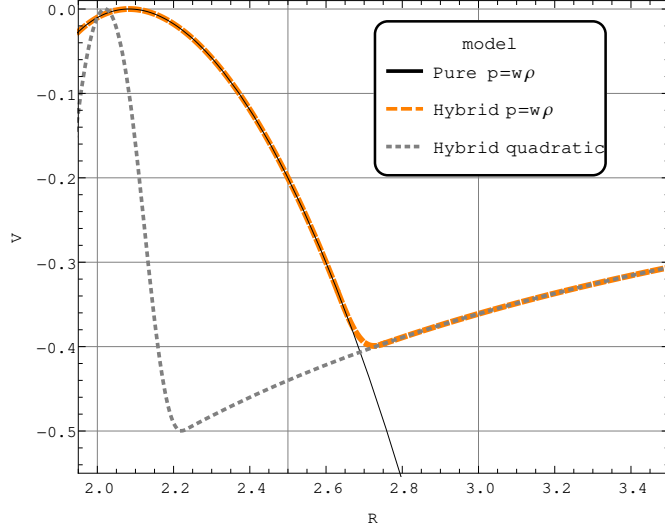


FIG. 3. The effective potentials $V(R)$ are plotted with solid, long-dashed, and short-dashed lines for the pure $p = w\rho$ with $w = 1$, hybrid $p = w\rho$ with $w = 1$, and hybrid quadratic models with $(\epsilon, \beta) = (10^{-1}, 0.5)$, respectively.

A. Pure $p = w\rho$ model

When the EOS is $p = w\rho$, where p is the surface pressure, ρ is the surface energy density, and w is a constant, the conservation of the kinetic energy of the shell is given by

$$\left(\frac{dR}{d\tau}\right)^2 + V(R) = 0 \quad \text{with} \quad V(R) = 1 - \frac{M}{R} - \left(\frac{m}{2R^{2w+1}}\right)^2 - \left(\frac{MR^{2w}}{m}\right)^2, \quad (5.1)$$

where m is a conserved quantity of the shell. This equation comes from the junction condition of the second fundamental form and the derivation of the potential is delegated to Appendix A. The equation for extremal values is given by $dV/dR = 0$. For $w > 0$, there is a single extremum, for which the radius $R = R_f$ is given by

$$\frac{R_f}{M} = \left[\frac{1 + 2w}{4w} \left(\frac{m}{M^{1+2w}} \right)^2 \right]^{1/(1+4w)} \quad (w > 0). \quad (5.2)$$

Since there is no extremum for $w \leq 0$, we concentrate on $w > 0$. This single extremum gives a global maximum of $V(R)$. By substituting Eq. (5.2) into $V(R_f)$ given by Eq. (5.1), we obtain $V(R_f) = 1 - (1 + 4w)^2(4w)^{-1}(1 + 2w)^{-1}R_f^{-1}M$. From the staticity condition $V(R_f) = 0$, R_f can also be written by

$$\frac{R_f}{M} = 2 + \frac{1}{4w(1 + 2w)}. \quad (5.3)$$

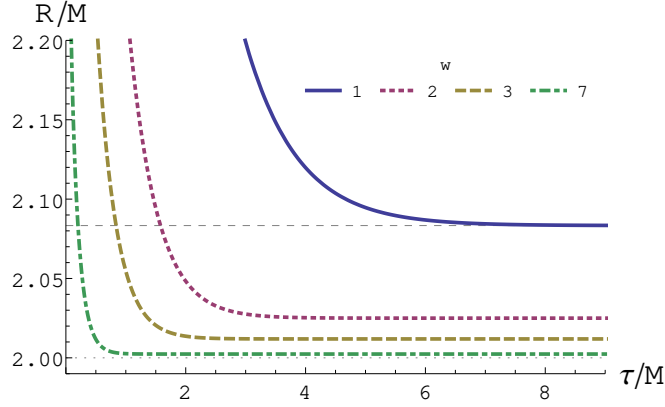


FIG. 4. The radius R of the shell with the EOS $p = w\rho$ is plotted as a function of τ for different values of w in the pure $p = w\rho$ model. The value $w = 1$ is the case where the dominant energy condition is marginally satisfied. In this case, the radius approaches $(25/12)M \simeq 2.08M$, which is plotted with the dashed straight line. For $w > 1$, where the dominant energy condition is violated, the larger the value of w , the closer to $2M$ the final radius.

The combination of Eqs. (5.2) and (5.3) gives a relation between m and w as

$$\frac{m}{M^{1+2w}} = \frac{(1+4w)^{1+4w}}{(4w)^{2w}(1+2w)^{1+2w}} =: m_f. \quad (5.4)$$

Under the above conditions, there is a unique static solution at $R = R_f$. The time evolution of the shell, which is collapsing at $R > R_f$, approaches this unstable static radius $R = R_f$.

Since R_f is a monotonically decreasing function of w as is seen from Eq. (5.3), as long as we respect energy conditions (the null, weak, dominant and strong energy conditions), i.e., $0 < w \leq 1$, R_f has its minimum $(25/12)M \simeq 2.0833M$ at $w = 1$. On the other hand, R_f approaches $2M$ as $w \rightarrow \infty$. Figure 4 shows the time evolution of the shell with different values of w , which is obtained by integrating Eq. (5.1) with Eq. (5.4).

For $w \gg 1$, R_f and m_f are approximately given by

$$\frac{R_f}{2M} - 1 \simeq \left(\frac{1}{4w}\right)^2, \quad m_f \simeq 2^{1+2w}. \quad (5.5)$$

The behavior of the shell near the final radius R_f is obtained by using the Taylor expansion of $V(R)$ around $R = R_f$. Since $V(R_f) = V'(R_f) = 0$, Eq. (5.1) reduces to $\dot{R}^2 \simeq -V''(R_f)(R - R_f)^2/2$. For a contracting shell for $w \gg 1$, this equation can be integrated to give

$$R - R_f \simeq D e^{-w\tau/M}, \quad (5.6)$$

where D is a constant of integration.

We should also note that since $V(R) \rightarrow -\infty$ as $R \rightarrow \infty$, the speed of the shell approaches that of light with respect to the observer at $r = \text{const.}$ and, hence, it approaches not the timelike infinity but the null infinity. Thus, the shell emerges from the past null infinity for the dynamics collapsing from infinity to $R = R_f$ as depicted in Fig. 5 (a).

As defined in Ref. [13, 14] and Paper I [12], the parameter ϵ controls the closeness of the final static radius to the horizon radius as

$$\frac{R_f}{2M} - 1 = \epsilon^2. \quad (5.7)$$

Therefore, for $w \gg 1$, Eqs. (5.5), (5.6), and (5.7) imply that this model in late times falls into model A with $\epsilon = 1/(4w)$ and $\sigma = 1/(4\epsilon M)$.

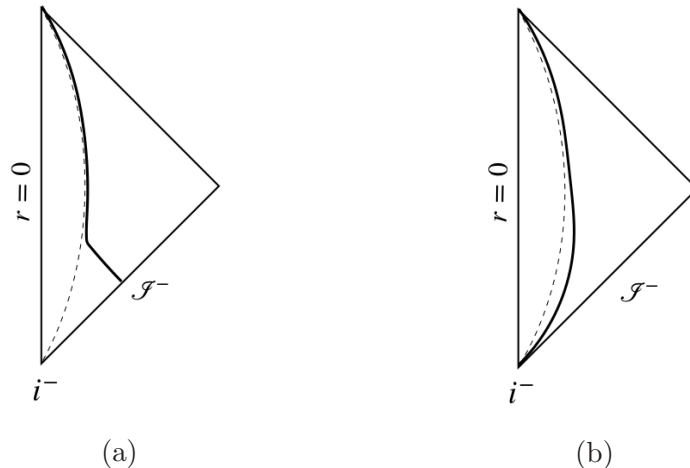


FIG. 5. (a) The conformal diagram for a collapsing shell in the pure $p = w\rho$ model. The thick curve depicts the motion of the shell starting from the past null infinity \mathcal{I}^- . The shell asymptotically approaches the final static radius R_f , which is slightly larger than $2M$. The timelike curve $r = R_f$ is depicted by the dotted line. (b) Same as (a) but for a collapsing shell starting from the past timelike infinity i^- , which is realized in the hybrid models.

B. Hybrid $p = w\rho$ model

As seen in Sec. V A, a collapsing shell with $p = w\rho$ emerges from the past null infinity. However, in astrophysically realistic situations, the star begins to collapse from a state nearly in free fall or in equilibrium. Therefore, we here introduce concrete models where the collapsing shell starts

from the past timelike infinity. The qualitative analysis of this picture without specific model is studied in detail in Paper I [12] and in Sec. IV in the current paper. To construct concrete pedagogical models, we look for an EOS for a collapsing shell which falls from a static state at the infinity and approaches the final radius which is close to its horizon radius. Since no physical EOS realizing such a dynamics is known to our knowledge, we reconstruct the EOS from the shape of the effective potential for the desired dynamics, instead of specifying the explicit form of EOS. Once the potential is specified, the corresponding EOS is determined through Eqs. (A5) and (A6).

Let $V_w(R)$ be the potential of a shell with $p = w\rho$ derived in the previous section and $V_0(R)$ be the potential of a dust shell falling from a static state at $R = \infty$. For our purpose, we connect $V_w(R)$ and $V_0(R)$ with an interpolating function $V_{\text{smooth}}(R)$ as

$$V(R) = \begin{cases} V_w(R) := 1 - M/R - m_f^2 M^{2+4w} / (4R^{2+4w}) - R^{4w} / (m_f^2 M^{4w}) & (R \leq R_s - l) \\ V_{\text{smooth}}(R) & (R_s - l \leq R \leq R_s + l), \\ V_0(R) := -M/R - M^2 / (4R^2) & (R \geq R_s + l) \end{cases}, \quad (5.8)$$

where $V_{\text{smooth}}(R)$ is a quintic function interpolating between V_w and V_0 so that V , V' and V'' are continuous. R_s is defined through $V_w(R_s) = V_0(R_s)$ so that it corresponds to the intersection between $V_w(R)$ and $V_0(R)$. Then, R_s is obtained as $R_s = m_f^{1/(2w)} M$. l determines the domain of the interpolating function $V_{\text{smooth}}(R)$ and is chosen as $l = (R_s - R_f)/A$ with a constant $A \geq 2$.¹ We note that because the shell falls from the static state at $R = \infty$ in this effective potential, it emerges from the past timelike infinity as depicted in Fig. 5 (b). From Eqs. (A5) and (A6), the surface density ρ and the ratio p/ρ for different values of w were numerically calculated and are summarized in Fig. 6 for $w = 1, 3, 10, 20$ and 30 . One can see that in each case, as ρ monotonically increases, p/ρ is kept 0 first, jumps from 0 to w very rapidly at some moment, and then is kept w afterwards. This is because this model is identical to the dust shell for $R \geq R_s + l$, the pure $p = w\rho$ shell model for $R < R_s - l$, and something smoothly connecting these two regimes for $R_s - l \leq R < R_s + l$ as discussed in Sec. V A.

¹ We have numerically calculated the time evolution of the power of radiation for different values of A in the range $2 \leq A \leq 10$ and found that the difference in the obtained result is very little under the two hybrid potentials given by Eq. (5.8) and Eq. (5.9), except for that the larger value of A caused numerical difficulty in the latter case. So, for the numerical results presented in this paper, we fix A to $A = 10$ and $A = 2$ for the potentials Eq. (5.8) and Eq. (5.9), respectively.

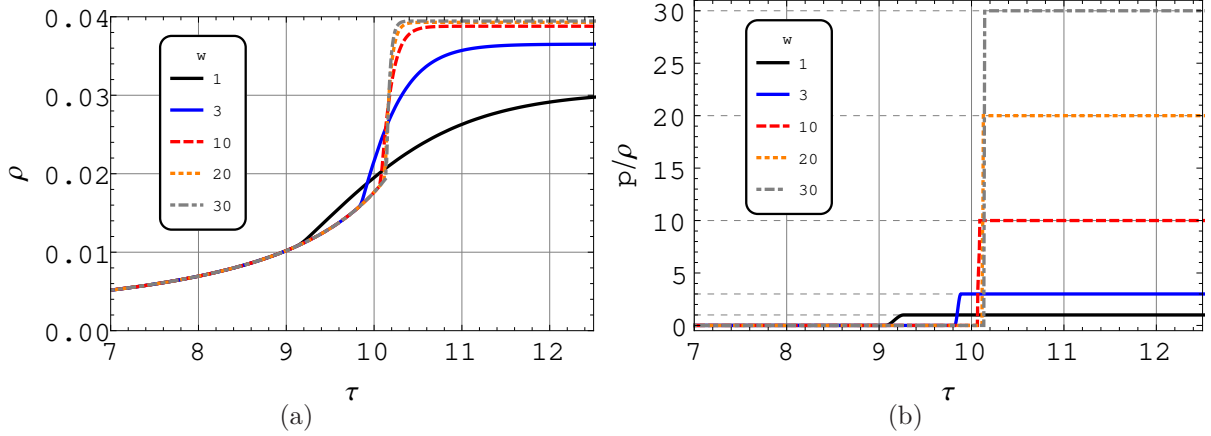


FIG. 6. The time evolution of (a) the surface density ρ and (b) the ratio p/ρ in the hybrid $p = w\rho$ model for $w = 1, 3, 10, 20$, and 30 . The surface density ρ monotonically increases and then approaches constant as the shell slows down to the final static radius. For each value of w , the ratio p/ρ is kept 0 first and then rapidly shifted to w at some moment. Then, the ratio p/ρ is kept w after the transition.

C. Hybrid quadratic model

Inspired from the hybrid $p = w\rho$ potential in the previous subsection, we next consider the following potential:

$$V(R) = \begin{cases} V_q(R) := -\sigma^2(R - R_f)^2/M^2 & (R \leq R_s - l) \\ V_{\text{smooth}}(R) & (R_s - l \leq R \leq R_s + l) \\ V_0(R) = -M/R - R^2/(4M^2) & (R \geq R_s + l) \end{cases}, \quad (5.9)$$

where $V_{\text{smooth}}(R)$ is, as in the hybrid $p = w\rho$ potential model, a quintic function smoothly interpolating $V_q(R)$ and $V_0(R)$. In other words, the whole potential is obtained by connecting the quadratic function and the dust potential with an interpolating function. Since R_f and σ are related to ϵ and β through $R_f = 2M(1 + \epsilon^2)$ and $\sigma^{-1} = 2M\epsilon^{2\beta}$, we can instead regard ϵ and β as free parameters. The larger value of σ with fixed R_f implies the larger value of β with fixed ϵ , corresponding to more squashed quadratic potential around $R = R_f$.

The time evolution of the surface density ρ and the ratio p/ρ for $(\epsilon, \beta) = (10^{-1}, 0.5), (10^{-1.5}, 0.5), (10^{-1.8}, 0.5), (10^{-1}, 0.9)$, and $(10^{-1}, 1)$ is shown in Fig. 7. The surface density ρ follows its evolution of the dust shell and then shifts to that of the shell with $p = w\rho$. The final value is determined by ϵ , while the time scale of the transition is determined by $\sigma^{-1} = 2M\epsilon^{2\beta}$. The ratio p/ρ begins with zero, increases to a maximum value, turns to decrease, and ends with some positive value

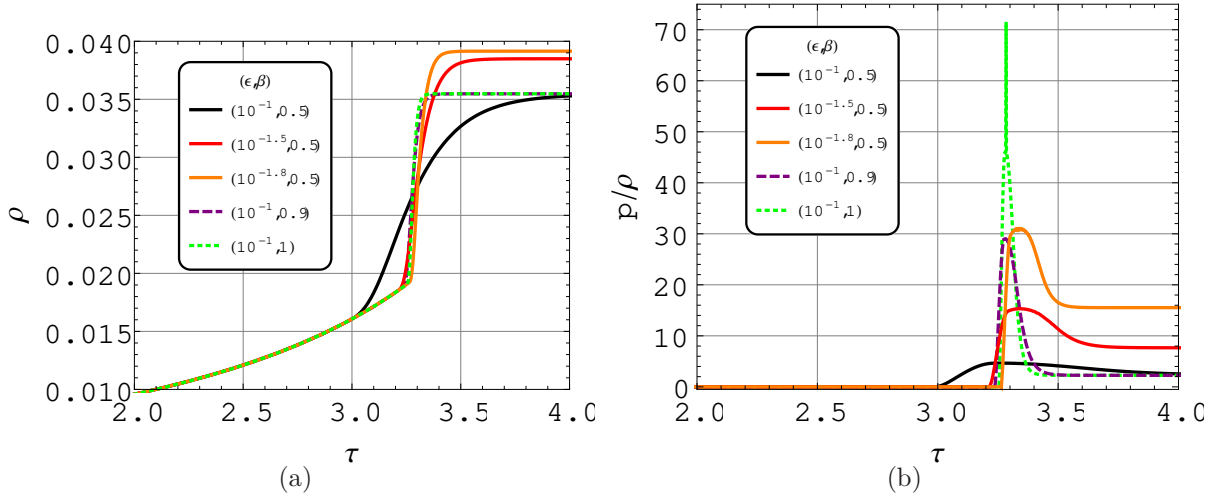


FIG. 7. The time evolution of (a) the surface density ρ and (b) the ratio p/ρ in the hybrid quadratic model for $(\epsilon, \beta) = (10^{-1}, 0.5)$, $(10^{-1.5}, 0.5)$, $(10^{-1.8}, 0.5)$, $(10^{-1}, 0.9)$, and $(10^{-1}, 1)$. The surface density ρ monotonically increases and then approaches constant as the shell slows down to the final static radius. The final static radius is determined by ϵ , while the time scale of the transition is determined by $\sigma^{-1} = 2M\epsilon^{2\beta}$. For each case, the ratio p/ρ is kept 0 first and then rapidly increased to some maximum value at some moment. Then, it turns to decrease and approaches the final value determined by ϵ .

determined by ϵ . The maximum value of the ratio is larger for the smaller value of ϵ and the larger value of β , while the final value is larger for the smaller value of ϵ but independent from β . All of the EOSs shown in both Figs. 7 (a) and (b) are thermodynamically unstable in the regime where $dp/d\rho < 0$.

VI. PARTICLE CREATION: A NUMERICAL ANALYSIS

A. Hybrid $p = w\rho$ transmissive model

Using Eqs. (2.1) and (2.4), we numerically calculated $\kappa(u)$ and then $P(u)$ with $\delta = 0$ for each dynamical model with the transmissive boundary condition. We present the numerical result in the hybrid models introduced in Sec. V.

Figure 8 shows the numerical result for the power of radiation in the hybrid $p = w\rho$ model with the transmissive boundary condition. Figure 8 (a) shows the time evolution of the power for $w = 1, 10, 20$, and 30 . The horizontal axis denotes u normalized by M . The power plotted are normalized by the power of the standard Hawking radiation $P_H := (48\pi)^{-1}(16M^2)^{-1}$. From

this figure, we find that there are two major peaks for each value of w . The first peak is emitted immediately after the shell gets very close to the final radius, while the second peak is much later. Figures 8 (b) and (c) are the enlarged figures of the first peaks for the different values of w and of the second peak for $w = 10$, respectively, where the enlarged areas are indicated with the rectangles of dashed lines in Fig. 8 (a). In Fig. 8 (b), we can see that the power first gradually increases in time, which corresponds to the rise of THR. Then, this rise of THR is suddenly interrupted before it reaches P_H . The larger the value of w , the later the time of the interruption. No significant bump is seen after the interruption of THR in Fig. 8 (b) except for $w = 1$, for which the second peak already appears in Fig. 8 (b). In Fig. 8 (c), we can see the time evolution of the power at the second peak for $w = 10$. The power is first negligibly small after the first peak. Then, it suddenly rises nearly to P_H very quickly and then decays in the time scale of a few tens of M . This time profile of the second peak is common to the different values of w . The second peak is associated with negative κ according to the qualitative analysis in Paper I. We observe that the peak values increase as w is increased, although P does not exceed P_H and remains as strong as P_H at most even for the larger values of w . The time interval between the two radiation peaks, Δu , increases as ϵ is decreased. In Fig. 8 (d), we plot the relation between the time interval of the two peaks, Δu , and w . The time interval Δu increases as w is increased. We also plot the relation $\Delta u \simeq 16wM$ with a solid line in the same figure. This relation can be derived from $\Delta u \simeq 4M/\epsilon$ obtained in Paper I [12] and $\epsilon = 1/(4w)$. We can see that the numerical result is in good agreement with the relation $\Delta u \simeq 16wM$.

B. Hybrid quadratic transmissive model

Figures 9 and 10 show the numerical result in the hybrid quadratic potential given by Eq. (5.9). Recall that the two parameters of this potential R_f and σ can also be parameterize by two non-dimensional parameters ϵ and β with $R_f = 2M(1 + \epsilon^2)$ and $\sigma^{-1} = 2M\epsilon^{2\beta}$.

First, we see the ϵ -dependence of the power of radiation in Fig. 9. Figure 9 (a) shows the time evolution of the power of radiation for $\epsilon = 10^{-1}$, $10^{-1.3}$, and $10^{-1.6}$, where $\beta = 0.5$ is fixed. We can see that there are two bursts, the first one exceeded by the second one. The peak values of the both increase as ϵ is decreased, although they still remain of the order of P_H . Figures 9 (b) and (c) are the enlarged figures of the first peaks for the different values of ϵ and of the second peak for $\epsilon = 10^{-1}$, respectively, where the enlarged areas in Figure 9 (a) are indicated with the rectangles of dashed lines. In Fig. 9 (b), we can see that the rise of THR is suddenly interrupted before it

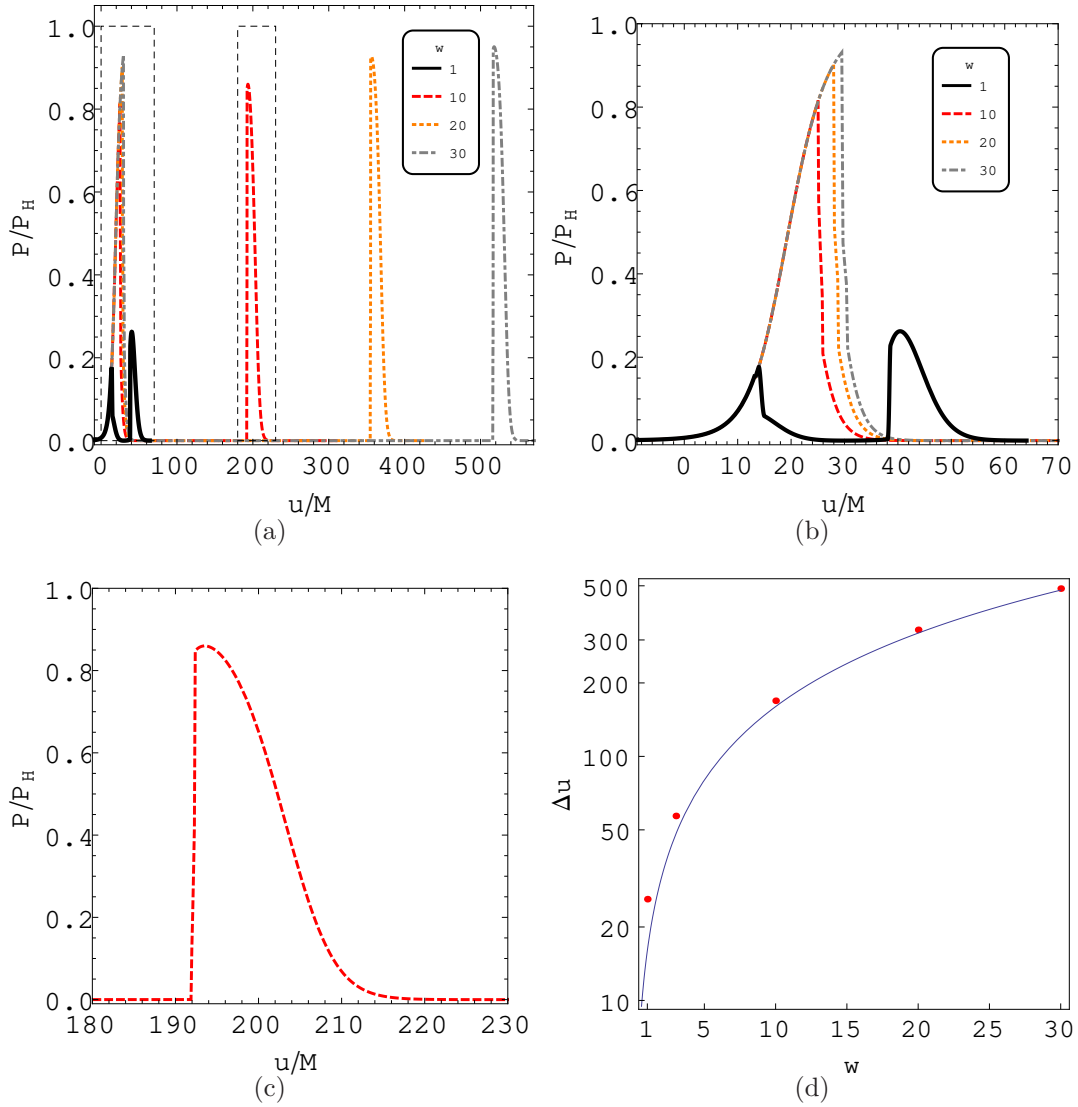


FIG. 8. The power of radiation in the hybrid $p = w\rho$ model with the transmissive boundary condition. (a) shows the time evolution of the power for $w = 1, 10, 20$, and 30 . (b) is the enlargement of the first-peak region indicated by the left rectangle of dashed lines in (a). (c) is the enlargement of the second-peak region for $w = 10$ indicated by the right rectangle of dashed lines in (a). (d) shows the relation between Δu and w for $w = 1, 3, 10, 20$, and 30 , where Δu is the time interval of the two peaks. The analytic formula $\Delta u = 16wM$ is also plotted with a solid line in (d).

reaches P_H . The smaller the value of ϵ , the later the time of the interruption. Unlike in the hybrid $p = w\rho$ model, we can see a small bump after the THR is interrupted. In fact, κ first increases nearly to the Hawking value κ_H , then decreases, crosses zero, and becomes negative. The negative value of κ is due to the braking of the collapse. This is discussed in Paper I, although this fine structure is omitted in the schematic figures, Figs. 5 and 6 in Paper I [12]. As the brake ceases,

the value of κ approaches zero. In Fig. 9 (c), we can see the time evolution of the power at the second peak. Its feature is similar to that in the hybrid $p = w\rho$ model except for that the value of the second peak is significantly larger than P_H . The peak value is larger and the time scale of the decay is longer for the smaller value of ϵ . The second peak is associated with negative κ according to the qualitative analysis in Paper I [12]. The interval between the two bursts is plotted as a function of ϵ for fixed $\beta = 0.5$ in Fig. 9 (d), from which we can see that the numerical result agrees well with the relation $\Delta u = 4M/\epsilon$ derived by the qualitative analysis in Paper I [12].

Next, we see the β -dependence shown in Fig. 10. In Fig. 10 (a), we plot the numerical result for the time evolution of the power for different values of β , while $\epsilon = 0.1$ is fixed. This corresponds to changing σ while fixing R_f . In this case, the situation drastically changes from the case of $\beta = 0.5$. We can see that the values of the both peaks can be much greater than P_H for $\beta > 0.5$. The larger the value of β , the larger both the first peak and second peak. Figures 10 (b) and (c) are the enlarged figures of the first peaks and second peaks, respectively, where the enlarged areas in Fig. 10 (a) are indicated with the rectangles of dashed lines. In Fig. 10 (b), we can see that the THR is suddenly interrupted and the power decreases to zero. Then, the power turns to increase and reaches the first peak, which is much larger than P_H . This first peak is associated with negative κ due to the braking of the collapse. After the first peak, the power soon decays to a negligibly small value. In Fig. 10 (c), we can see the detailed time evolution of the second peak, which is associated with negative κ . Figure 10 (d) shows the relation between the values of the two peaks and β for fixed $\epsilon = 0.1$. From this figure, we can see that the first and the second peaks are proportional to $P/P_H = \epsilon^{2(1-2\beta)} = (\epsilon \cdot 2M\sigma)^2$ for $\beta \geq 0.5$, which is derived as Eq. (6.12) in Paper I [12] and plotted by a solid line in Fig. 10 (d). We can see that β together with ϵ controls the strength of the peak power. The peak value becomes larger for the smaller value of ϵ and the larger value of β . Within our numerical result, the strongest burst was $P/P_H \simeq 800$ as the second peak for $(\epsilon, \beta) = (0.1, 1.1)$. We can see from Fig. 10 (a) that the time interval between the two peaks for the different values of β with fixed ϵ is almost constant, which is consistent with the general relation $\Delta u = 4M/\epsilon$.

To summarize, the closer the final static radius to the horizon radius, the longer the interval between the first and second bursts, while the more squashed the parabolic potential or the stronger the brake, the stronger both the first and second bursts.

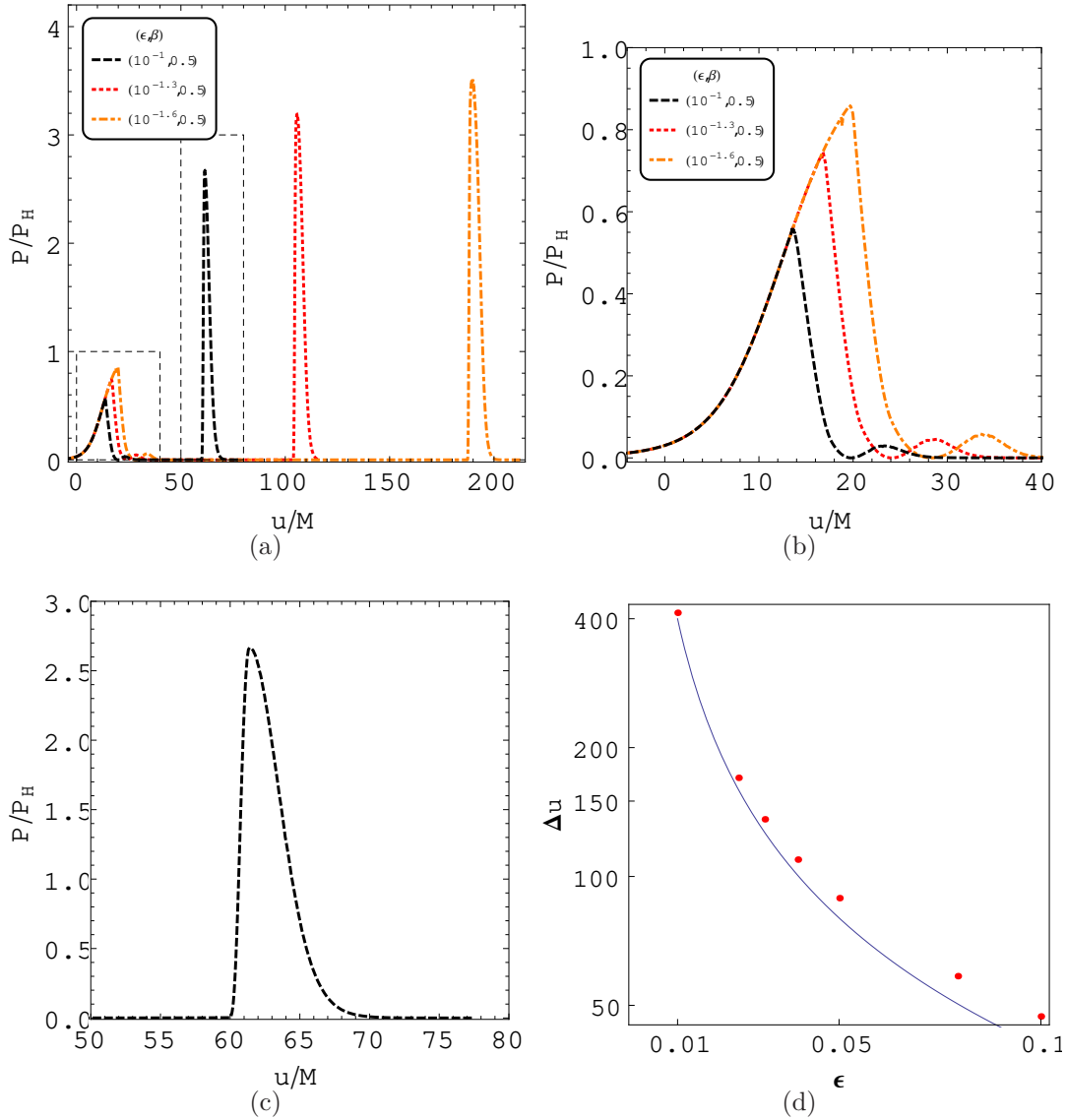


FIG. 9. The power of radiation in the hybrid quadratic model with the transmissive boundary condition: ϵ -dependence. (a) shows the time evolution of the power for $\epsilon = 10^{-1}, 10^{-1.3}$, and $10^{-1.6}$, where $\beta = 0.5$ is fixed. (b) is the enlargement of the first-peak region indicated by the left rectangle of dashed lines in (a). (c) is the enlargement of the second-peak region indicated by the right rectangle of dashed lines in (a) for $(\epsilon, \beta) = (10^{-1}, 0.5)$. (d) shows the relation between Δu and ϵ for different values of ϵ , where $\beta = 0.5$ is fixed. The analytic formula $\Delta u = 4M/\epsilon$ is plotted with a solid line in (d).

C. Hybrid $p = w\rho$ reflective model

Using Eqs. (2.1) and (2.9), we numerically calculated $\kappa(u)$ and then $P(u)$ with $\delta = 0$ for each dynamical model with the reflective boundary condition. Here, we present the numerical result for

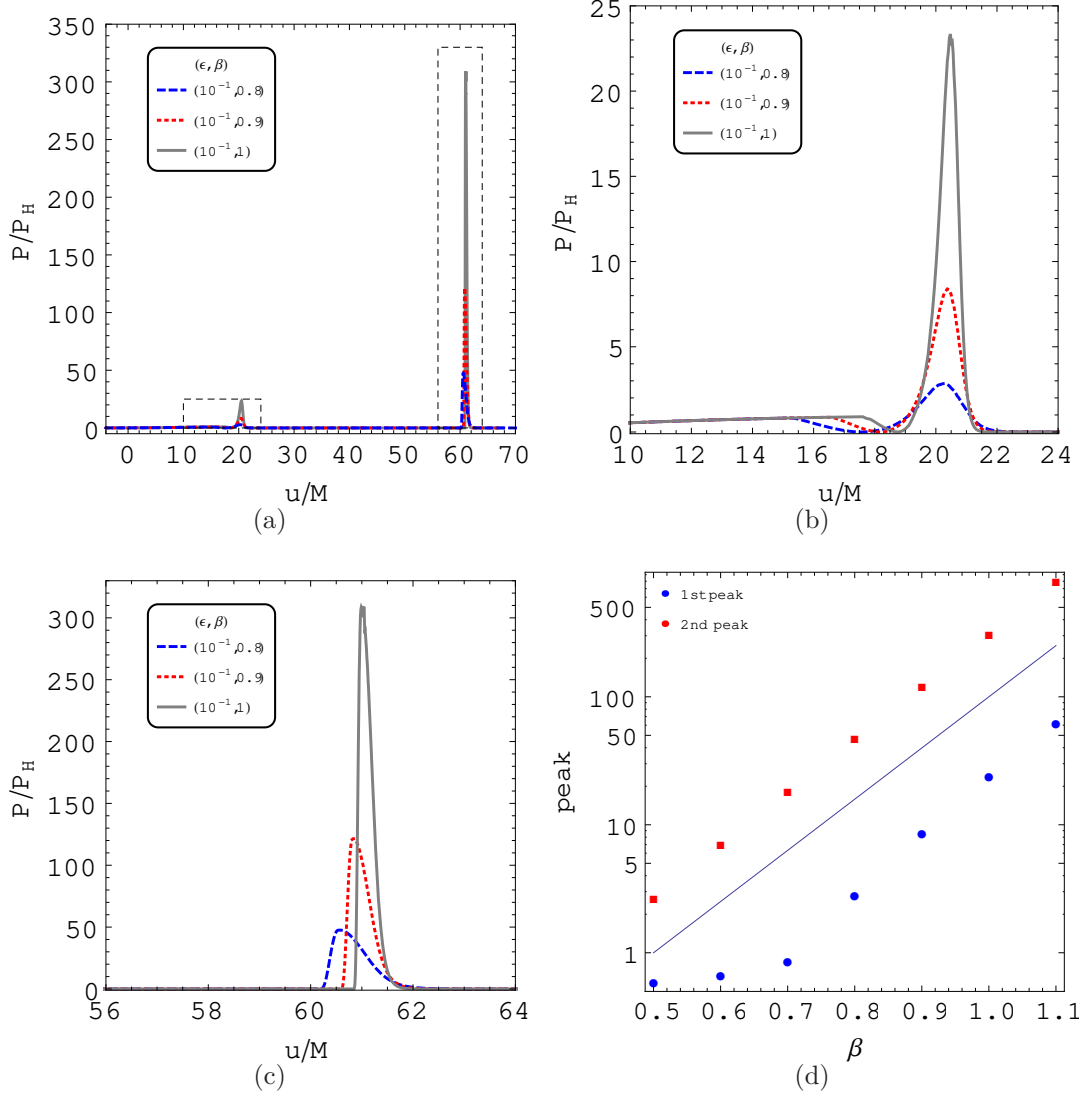


FIG. 10. The power of radiation in the hybrid quadratic model with the transmissive boundary condition: β -dependence. (a) shows the time evolution of the power for $\beta = 0.8, 0.9$, and 1.0 , where $\epsilon = 10^{-1}$ is fixed. (b) is the enlargement of the first-peak region indicated by the left rectangle of dashed lines in (a). (c) is the enlargement of the second-peak region indicated by the right rectangle of dashed lines in (a). (d) shows the relation between the values of the two peaks normalized by P_H and β with $\epsilon = 0.1$. The analytic formula $P/P_H = \epsilon^{2(1-2\beta)}$ is plotted with a solid line in (d).

the power evolution emitted from a collapsing reflective surface. Note that to calculate the power of radiation, we do not have to specify the internal structure of the collapsing body but only the dynamics of the reflective surface. Here, however, just for convenience, we continue to use the same terminology to refer to the dynamics of the reflective surface as if it is a hollow spherical

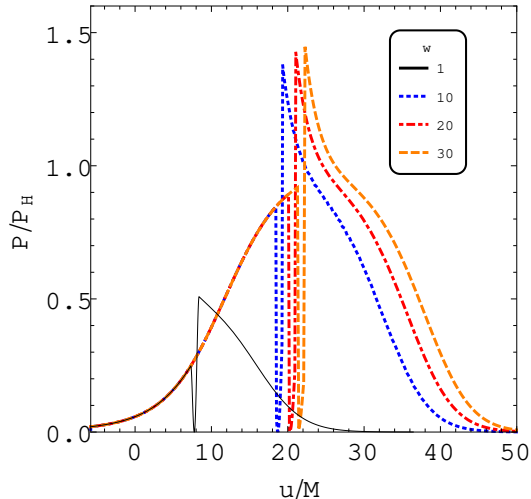


FIG. 11. The time evolution of the power of radiation in the hybrid $p = w\rho$ potential with the reflective boundary condition for $w = 1, 10, 20,$ and 30 .

shell.

Figure 11 shows the numerical result for the power evolution in the hybrid $p = w\rho$ model with $w = 1, 10, 20,$ and 30 for the reflective boundary condition. We can clearly see that the THR first rises and is suddenly interrupted to zero in a time scale much shorter than M . The THR is nearly complete for $w \gtrsim 10$, while it is far from complete for $w = 1$. After the THR is interrupted in the very short time scale, we can see a burst arises in the same short time scale to the value as strong as P_H . This post-Hawking burst is associated with negative κ and decays in the time scale of a few tens of M . The time evolution is delayed for larger values of w but it is not very sensitive for $w \gtrsim 10$. This is consistent with the qualitative analysis showing the dependence $\sim \log \epsilon^{-1} \sim \log w$ of the duration of the THR in terms of u as is discussed in Sec. III. The burst is single and there is no further burst. This is in contrast to the transmissive case, where such a burst does not appear immediately after the THR as discussed in Sec. VI A.

D. Hybrid quadratic reflective model

Figure 12 shows the numerical result for the power of radiation from a reflective surface in the hybrid quadratic model. Figure 12 (a) shows the time evolution of the power for $\epsilon = 10^{-1}, 10^{-1.3},$ and $10^{-1.6}$ with $\beta = 0.5$. We can see that the rise of THR is suddenly interrupted in a short time scale. A peak appears immediately after the interruption of THR. This post-Hawking burst is associated with negative κ and decays in the time scale of a few tens of M . The smaller the

value of ϵ , the later the interruption of THR and the appearance of the post-Hawking burst. This is in contrast to the transmissive case, where there is only a small bump immediately after the interruption of THR as discussed in Sec. VI B. Figure 12 (b) shows the power evolution for $\beta = 0.8, 0.9, \text{ and } 1.0$ with $\epsilon = 0.1$. We can see that the peak value is much larger than P_H for these values of β . Figure 12 (c) shows the enlarged figure of the peaks, where the enlarged region is indicated by the rectangle of dashed lines in Fig. 12 (b). We can see that the THR first rises but is suddenly interrupted. The power drops to zero, turns to increase, rises to a peak, and then decays to zero. The β -dependence of the peak value for $\epsilon = 0.1$ is plotted in Fig. 12 (d), in which the formula $P/P_H = \epsilon^{2(1-2\beta)} = (\epsilon \cdot 2M\sigma)^2$, which is derived in Sec. IV C, is also plotted by a solid line. We can see that the numerical result is in good agreement with the formula. As in the transmissive surface, both ϵ and β control the peak values of the power, while ϵ delays the single peak although it is not very sensitive for $\epsilon \lesssim 10^{-1}$.

To summarize the numerical result for the reflective surface, we find that after the power initially rises gradually as the THR develops, the power suddenly vanishes in a very short time scale. This moment of the vanishing power corresponds to the change of the sign of κ from positive to negative. After this interruption of THR, a burst arises associated with negative κ , exceeds P_H and decays in the time scale of a few tens of M . This post-Hawking burst is stronger than that in the transmissive case for the same collapse dynamics. On the other hand, it is interesting that the strength and the duration of each burst in the reflective case is not so different from the first burst in the transmissive case for the same dynamics of the shell. The crucial difference is that the reflective surface emits a single burst, while the transmissive emits two.

VII. DISCUSSION AND CONCLUSION

We have studied particle creation in the collapse to an ultracompact object with two different boundary conditions at the surface of the object and with two different matter or potential models for the dynamics of the surface. In Paper I, the authors studied a collapsing transmissive hollow shell. They analytically showed the existence of the THR followed by a couple of bursts separated each other by the long time interval and how the strength and duration of the bursts depend on the dynamics of the shell. In the current paper, we have also studied a collapsing reflective surface and analytically showed the existence of the THR followed by a single burst and how the strength and duration of the burst depend on the dynamics of the surface. We have found that the numerical result confirms the analytical result. Within our numerical result, the closer the

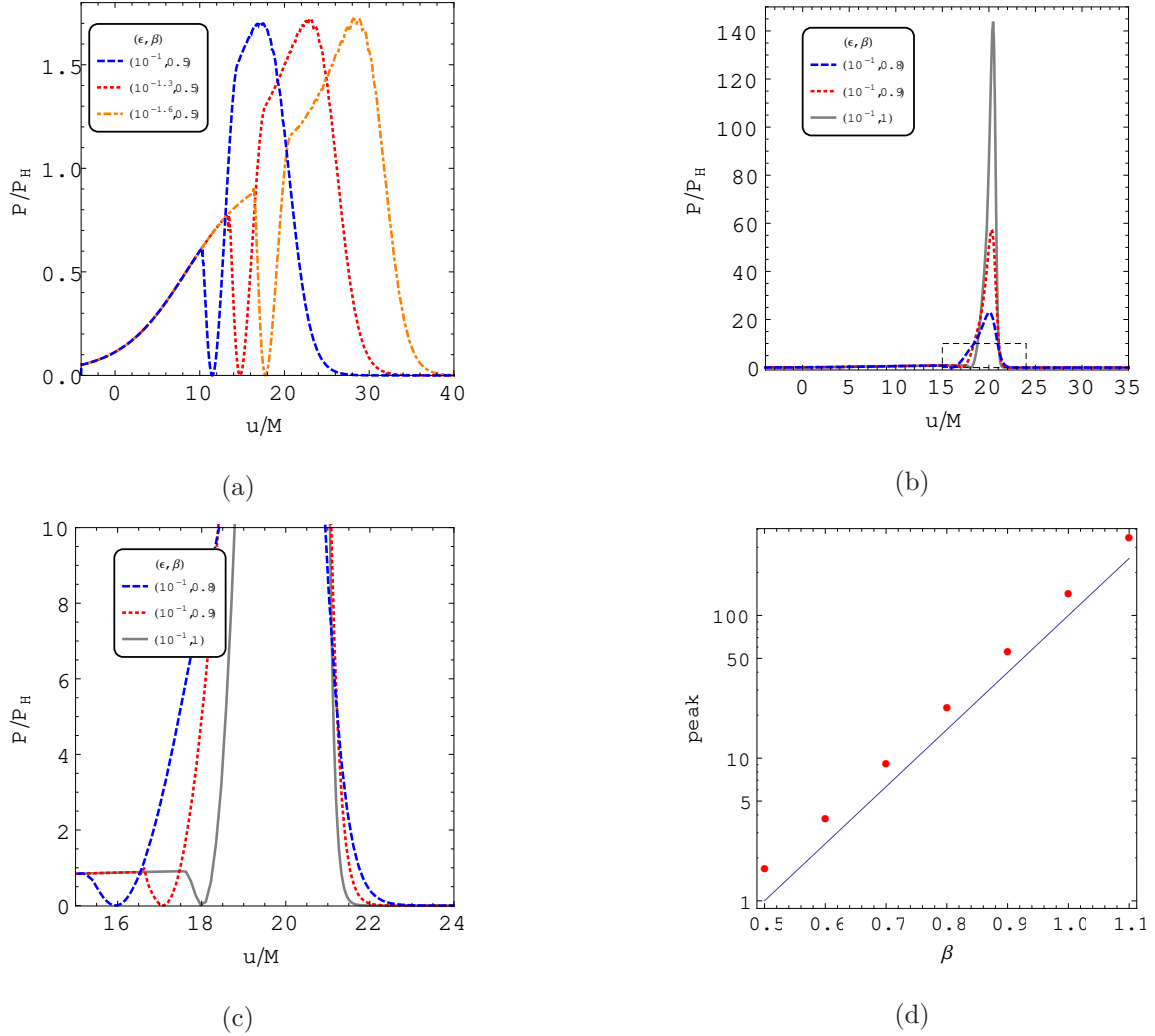


FIG. 12. The power of radiation in the hybrid quadratic model with the reflective boundary condition. (a) shows $P(u)$ for $\epsilon = 10^{-1}$, $10^{-1.3}$, and $10^{-1.6}$ with $\beta = 0.5$. (b) shows $P(u)$ for $\beta = 0.8$, 0.9 , and 1.0 with $\epsilon = 0.1$. (c) is the enlargement of the region indicated by the rectangle of dashed lines in (b). (d) shows the relation between the peak value and β with $\epsilon = 0.1$. The analytic formula $P/P_H = \epsilon^{2(1-2\beta)}$ is also plotted with a solid line in (d).

final static radius to the horizon radius, the larger the peak values of the power. If the EOS of the matter is described by $p = w\rho$ in its final stage of evolution, the power of the two bursts remain of the order of that of the Hawking radiation at most. On the other hand, we have successfully constructed a concrete model described by a quadratic potential in its final stage of evolution that emits a burst of radiation which is much stronger than the Hawking radiation. It depends on the boundary condition on the surface whether the burst is single or double. The present numerical result suggests that the EOS for the matter on the shell that emits bursts much stronger than the

Hawking radiation has a large maximum of the ratio p/ρ implying a thermodynamically unstable regime in the late-time phase of evolution, although further investigation is yet necessary to draw a general statement.

It should be noted that in the current model the formed ultracompact object is necessarily dynamically unstable. This is partly because the surface cannot stay at the local minimum of the effective potential but the local maximum if the energy of the shell is conserved during the collapse and partly because the effective potential of the shell connecting the Minkowski domain and the Schwarzschild domain cannot have a local minimum. On the other hand, the formation of a stable object as a result of gravitational collapse is possible if the system loses energy and if the interior is the de-Sitter spacetime. For example, Visser and Wiltshire [6] found that there are some physically reasonable EOSs for the transition layer that lead to stable gravastar configurations. Nakao, Yoo and Harada [9] presented the formation scenario of a stable gravastar after the emission of null shells from a timelike shell. In this context, the current analysis of toy models suggests a possible mechanism for a collapsing object to lose its energy by quantum particle creation and thus that a stable ultracompact object is possible as a result of gravitational collapse if the backreaction of particle emission is taken into account and if a non-empty interior gives the effective potential a local minimum.

We also discuss that the possibility of echoes in particle creation. Since we have adopted geometric optics approximation, the particle emission does not show any echoes. However, if the backscattering due to the effective potential is taken into account, scalar waves will be reflected due to the potential barrier around at $r = 3M$. This may induce echoes in particle creation both in the transmissive and reflective cases.

While the current work was being finalized, a preprint [20] appeared on the arXiv. Although the result of the current paper partially has some overlap with Ref [20], both papers are complementary to each other in other part.

ACKNOWLEDGMENTS

The authors are grateful to D. Miyata, V. Cardoso, K. Nakashi and T. Tanaka for their helpful comments. This work was partially supported by JSPS KAKENHI Grant Number JP19K03876 (T.H.).

Appendix A: Junction conditions

A singular, spherical and timelike hypersurface Σ (thin-shell) partitions the spacetime into the inner (−) and the outer (+) region. Each of the metric of the solutions can be, with the coordinates (t, r, θ, ϕ) , written by

$$ds_{\pm}^2 = -f_{\pm}(r_{\pm})dt_{\pm}^2 + f_{\pm}(r_{\pm})^{-1}dr_{\pm}^2 + r_{\pm}^2(\sin^2\theta d\theta^2 + d\phi^2) \quad \text{with} \quad f_{\pm}(r_{\pm}) = 1 - 2M_{\pm}/r_{\pm}, \quad (\text{A1})$$

where quantities with the plus sign (the minus sign) belong to the outer (inner) spacetime and M_{\pm} are the masses in the inner and outer regions, respectively. We construct a spacetime having a single thin-shell at Σ , on which the line element is given by $ds_{\Sigma}^2 = h_{ab}dy^a dy^b := -d\tau^2 + R(\tau)^2(\sin^2\theta d\theta^2 + d\phi^2)$, where $\{y^a\}$ are the intrinsic coordinates on Σ and are chosen as $y^i = (\tau, \theta, \phi)$. τ stands for the proper time on the shell Σ whose position is described by the coordinates $x^{\mu}(y^a) = (t(\tau), a(\tau), \theta, \phi)$. The equation of the surface Σ is given by $r_{\pm} = R(\tau)$. The unit normals n^{α} to Σ and basis vectors $e_a^{\alpha} := \partial x^{\alpha}/\partial y^a$ tangent to Σ are written by $n_{\alpha\pm} dx^{\alpha} = -\dot{R}dt + \dot{t}_{\pm}dr$, $u_{\pm}^{\alpha}\partial_{\alpha\pm} := e_{\tau\pm}^{\alpha}\partial_{\alpha\pm} = \dot{t}_{\pm}\partial_t + \dot{R}\partial_r$, $e_{\theta}^{\alpha}\partial_{\alpha} = \partial_{\theta}$, $e_{\phi}^{\alpha}\partial_{\alpha} = \partial_{\phi}$, so that $u^{\alpha}u_{\alpha} = -1$, $n_{\alpha}n^{\alpha} = 1$ and $u^{\alpha}n_{\alpha} = 0$ are satisfied, where the dot denotes the derivative with respect to τ . The junction conditions are written as $[h_{ab}] = 0$ and

$$8\pi S_{ab} = -[K_{ab}] + [K]h_{ab}, \quad (\text{A2})$$

where $K_{ab} := h_a^c h_b^d \nabla_c n_d$ is the extrinsic curvature, S_{ab} is the stress-energy tensor confined on a hypersurface Σ , and $[X] := (X^+ - X^-)|_{\Sigma}$. The constraint equations are given by

$$S_a^b{}_{|b} = -[T_{\alpha\beta}e_a^{\alpha}n^{\beta}], \quad (\text{A3})$$

$$\bar{K}^{ab}S_{ab} = [T_{\alpha\beta}n^{\alpha}n^{\beta}], \quad (\text{A4})$$

where $\bar{K}^{ab} := (K_+^{ab} + K_-^{ab})|_{\Sigma}/2$ and “ $|_a$ ” denotes the covariant derivative associated with the induced metric h_{ab} . From $[h_{ab}] = 0$, we obtain $\dot{t}_{\pm} := F_{\pm}/f_{\pm}(R)$, where $F_{\pm} := (f_{\pm}(R) + \dot{R}^2)^{1/2}$. The non-zero components of the extrinsic curvature are $K_{\tau}^{\tau\pm} = \dot{F}_{\pm}/\dot{R}$ and $K_{\theta}^{\theta\pm} = K_{\phi}^{\phi\pm} = F_{\pm}/R$. We take S_j^i as a perfect fluid form, $S_j^i = \text{diag}(-\rho, p, p)$ with the surface pressure p and the surface energy density ρ . Then, Eq. (A2) reduces to

$$-4\pi\rho = (F_+ - F_-)/R, \quad (\text{A5})$$

$$8\pi p = (\dot{F}_+ - \dot{F}_-)/\dot{R} + (F_+ - F_-)/R. \quad (\text{A6})$$

Eq. (A3) is explicitly written by

$$R\dot{\rho} = -2\dot{R}(p + \rho). \quad (\text{A7})$$

From Eq. (A7), ρ is solved as $\rho = \rho(R)$ when the EOS is given. If the inner region is flat and the outer is Schwarzschild with a mass M , by reducing Eq. (A5), we arrive $\dot{R}^2 + V(R) = 0$, where

$$V(R) := 1 - \frac{M}{R} - \left(\frac{M}{R}\right)^2 \frac{1}{(4\pi\rho R)^2} - (2\pi\rho R)^2. \quad (\text{A8})$$

Here, we assumed the shell takes a linear EOS, i.e., $p = w\rho$ with $w = \text{const}$. By combining Eqs. (A5) and (A6), we obtain

$$F_+ - F_- = C/R^{1+2w}, \quad (\text{A9})$$

where C is a constant of integration. Comparing Eq. (A5) and Eq. (A9), we can identify C as

$$-C = 4\pi\rho R^{2(w+1)} =: m, \quad (\text{A10})$$

where m is a constant. It should be noted that $4\pi R^2\rho^{1/(w+1)} = (4\pi)^{w/(w+1)}m^{1/(w+1)}$ can be identified with the conserved number of particles of which the shell consists. Thus, the effective potential of Eq. (A8) reduces to Eq. (5.1).

-
- [1] B. P. Abbott *et al.* [LIGO Scientific and Virgo Collaborations], Phys. Rev. Lett. **116** (2016) no.6, 061102 doi:10.1103/PhysRevLett.116.061102 [arXiv:1602.03837 [gr-qc]].
 - [2] B. P. Abbott *et al.* [LIGO Scientific and Virgo Collaborations], “Binary Black Hole Population Properties Inferred from the First and Second Observing Runs of Advanced LIGO and Advanced Virgo,” arXiv:1811.12940 [astro-ph.HE].
 - [3] K. Akiyama *et al.* [Event Horizon Telescope Collaboration], “First M87 Event Horizon Telescope Results. I. The Shadow of the Supermassive Black Hole,” Astrophys. J. **875** (2019) no.1, L1. doi:10.3847/2041-8213/ab0ec7
 - [4] V. Cardoso and P. Pani, “Testing the nature of dark compact objects: a status report,” arXiv:1904.05363 [gr-qc].
 - [5] P. O. Mazur and E. Mottola, “Gravitational vacuum condensate stars,” Proc. Nat. Acad. Sci. **101** (2004) 9545 doi:10.1073/pnas.0402717101 [gr-qc/0407075].
 - [6] M. Visser and D. L. Wiltshire, “Stable gravastars: An Alternative to black holes?,” Class. Quant. Grav. **21** (2004) 1135 doi:10.1088/0264-9381/21/4/027 [gr-qc/0310107].
 - [7] C. Barcelo, S. Liberati, S. Sonego, and M. Visser, “Fate of gravitational collapse in semiclassical gravity,” Phys. Rev. D **77** (2008) 044032 doi:10.1103/PhysRevD.77.044032 [arXiv:0712.1130 [gr-qc]].

- [8] M. Visser, C. Barcelo, S. Liberati, and S. Sonego, “Small, dark, and heavy: But is it a black hole?,” PoS BHGRS (2008) 010 [arXiv:0902.0346 [gr-qc]].
- [9] K. i. Nakao, C. M. Yoo and T. Harada, “Gravastar formation: What can be the evidence of a black hole?,” Phys. Rev. D **99** (2019) no.4, 044027 doi:10.1103/PhysRevD.99.044027 [arXiv:1809.00124 [gr-qc]].
- [10] S. W. Hawking, “Black hole explosions,” Nature **248** (1974) 30. doi:10.1038/248030a0
- [11] S. W. Hawking, “Particle Creation by Black Holes,” Commun. Math. Phys. **43** (1975) 199 Erratum: [Commun. Math. Phys. **46** (1976) 206]. doi:10.1007/BF02345020
- [12] T. Harada, V. Cardoso and D. Miyata, “Particle creation in gravitational collapse to a horizonless compact object,” Phys. Rev. D **99** (2019) no.4, 044039.
- [13] A. Paranjape and T. Padmanabhan, “Radiation from collapsing shells, semiclassical backreaction and black hole formation,” Phys. Rev. D **80** (2009) 044011 doi:10.1103/PhysRevD.80.044011 [arXiv:0906.1768 [gr-qc]].
- [14] K. Banerjee and A. Paranjape, “Semiclassical environment of collapsing shells,” Phys. Rev. D **80** (2009) 124006 doi:10.1103/PhysRevD.80.124006 [arXiv:0909.4668 [gr-qc]].
- [15] E. T. Akhmedov, H. Godazgar, and F. K. Popov, “Hawking radiation and secularly growing loop corrections,” Phys. Rev. D **93** (2016) no.2, 024029 doi:10.1103/PhysRevD.93.024029 [arXiv:1508.07500 [hep-th]].
- [16] N. D. Birrell and P. C. W. Davies, “Quantum Fields in Curved Space,” (Cambridge University Press, Cambridge, 1984), doi:10.1017/CBO9780511622632
- [17] L. H. Ford and L. Parker, “Creation of Particles by Singularities in Asymptotically Flat Space-Times,” Phys. Rev. D **17** (1978) 1485. doi:10.1103/PhysRevD.17.1485
- [18] C. Barcelo, S. Liberati, S. Sonego, and M. Visser, “Hawking-like radiation from evolving black holes and compact horizonless objects,” JHEP **1102** (2011) 003 doi:10.1007/JHEP02(2011)003 [arXiv:1011.5911 [gr-qc]].
- [19] S. Kinoshita and N. Tanahashi, “Hawking temperature for near-equilibrium black holes,” Phys. Rev. D **85** (2012) 024050 doi:10.1103/PhysRevD.85.024050 [arXiv:1111.2684 [hep-th]].
- [20] C. Barcelo, V. Boyanov, R. Carballo-Rubio and L. J. Garay, “Semiclassical gravity effects near horizon formation,” arXiv:1904.06558 [gr-qc].